Rolling Moments in a Trailing Vortex Flowfield

O. J. McMillan,* R. G. Schwind,* J. N. Nielsen,† and M. F. E. Dillenius*
Nielsen Engineering & Research, Inc., Mountain View, Calif.

Pressure distributions are presented which were measured on a wing in close proximity to a tip vortex of known structure generated by a larger, upstream semispan wing. Overall loads calculated by integration of these pressures are checked by independent measurements made with an identical model mounted on a force balance. Several conventional methods of wing analysis are used to predict the loads on the following wing. Strip theory is shown to give uniformly poor results for loading distribution, although predictions of overall lift and rolling moment are sometimes acceptable. Good results are obtained for overall coefficients and loading distribution by using linearized pressures in vortex-lattice theory in conjunction with a rectinlinear vortex. The equivalent relation from reverse-flow theory that can be used to give economic predictions for overall loads is presented.

Nomenclature

a_0 = three-dimensional lift-curve slope
$\mathcal{R}$ = aspect ratio of wing portion, Eq. (7)
b = wingspan
c = wing chord
c_l = section lift coefficient
c_{l_α} = section lift-curve slope
$(c_l)_{\text{roll}}$ = section lift coefficient for wing in steady roll, Eq. (8)
C_l = rolling-moment coefficient, $R/q_\infty bS$
$\hat{C}_l$ = rolling-moment coefficient for force model at zero angle of attack in absence of vortex; tare value
C_L = lift coefficient, $L/q_\infty S$
$\hat{C}_L$ = lift coefficient for force model at zero angle of attack in absence of vortex; tare value
C_p = pressure coefficient (based on corrected pressure), $(p-p_\infty)/q_\infty$
k = constant in model for leading-edge contribution to section lift, Eq. (4)
L = lift
p = static pressure corrected for pressure measured at same point on pressure model at zero angle of attack in absence of vortex; also roll angular velocity, positive right wing down
P = ratio of semiperimeter to span of wing portion, Eq. (7)
q_∞ = freestream dynamic pressure
r = radial distance from vortex centerline
R = rolling moment, positive right wing down
Re_c = Reynolds number based on the chord of the following wing
s = wing semispan, $b/2$
S = wing area, bc for rectangular wing
t = pseudo time coordinate, Eq. (1)
V_θ = tangential velocity in vortex, Eq. (2)
V_∞ = freestream velocity
w_v = component normal to wing of velocity due to vortex, Eqs. (5) and (6)
x,y,z = Cartesian coordinates with origin at the centerline of the leading edge of the following wing, Fig. 1
y_v,z_v = coordinates of the vortex center assuming that the presence of the wing causes no deflection
α = angle of attack
Γ = circulation of vortex at radius r, Eq. (1); positive for counterclockwise rotation
Γ_0 = strength of potential vortex; or circulation of vortex at large r
ν = pseudo viscosity, Eq. (1)

Subscripts

G = generating wing
l = lower wing surface
u = upper wing surface
v = vortex
∞ = freestream

Presented as Paper 77-670 at the AIAA 10th Fluid and Plasmadynamics Conference, Albuquerque, N. Mex., June 17-29, 1977; submitted July 18, 1977; revision received Jan. 23, 1978.

Index categories: Computational Methods; Jets, Wakes, and Viscid-Inviscid Flow Interactions.
*Research Engineer. Member AIAA.
†President. Fellow AIAA.

I. Introduction

THERE is considerable practical interest in the ability to calculate the loads induced on a wing surface in a freestream by a nearby streamwise vortex. For example, this ability is important in the analysis of the vortex hazard problem for a small aircraft operating in the wake of a larger aircraft. It is also central to the analysis of helicopter rotor systems and to the design of control or lifting surfaces for missiles or aircraft, if these surfaces are subject to concentrated vortices generated by the nose or by canards. Several investigators have formulated models for calculating induced loads of this type; varying levels of success have been achieved in terms of prediction of overall effects.

In spite of the fact that there is a voluminous literature on this subject, there exists a need for experimental data of sufficient detail and completeness to evaluate the theoretical methods. With the exception of the investigation of Ref. 1, the existing data lack either detailed measurements of the distribution of loading on the wing or knowledge of the structure of the approaching vortex; Ref. 1 deals with the case where the vortex-generating wing is at most of the same span as the following wing. Therefore, previous tests of theories (for cases where the vortex core is at all appreciable compared to the scale of the following wing) have been in terms of gross effects or have required critical assumptions with respect to the nature of the vortical flowfield involved.

In this paper a set of detailed measurements for the loading on the following wing is presented and analyzed where the vortex was generated by a larger wing. In the particular cases treated, the streamwise vortex was at various spanwise positions above (but close to) the following wing which was at zero angle of attack. Some standard methods of wing analysis are used to predict the loads on the following wing; com-

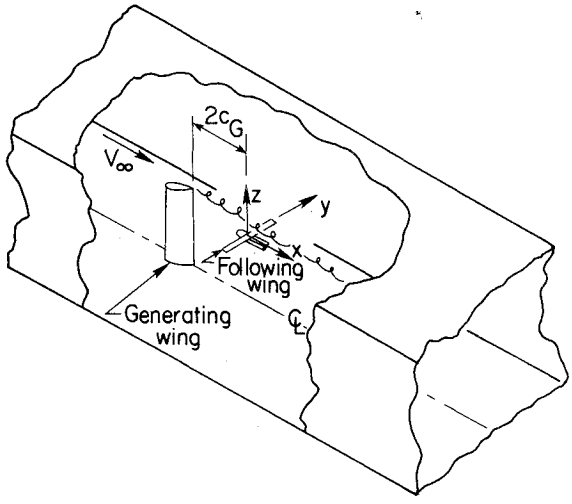

Fig. 1 Experimental arrangement.

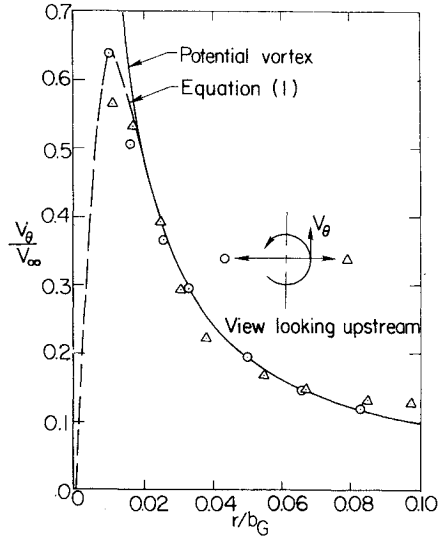

Fig. 2 Tangential velocity profile through vortex core (from Ref. 4) two chord lengths downstream of generating wing, $V_\infty = 24$ m/s, $\alpha_G = 12$ deg.

parisons with the measurements are made; and shortcomings of the methods are assessed. The loads were measured using pressure taps. To allow checking of the overall coefficients calculated by integration of the measured surface pressures, independent measurements were made using an identical model mounted on a force balance. Further details of this investigation are presented in Ref. 2.

II. Experimental Investigation

Apparatus and Instrumentation

The experiment was performed in the wind tunnel which is under the jurisdiction of the U.S. Army Air Mobility Research and Development Laboratory at the NASA Ames Research Center. This is a closed-circuit, atmospheric tunnel with a test section of rectangular cross section 2.1 m (7 ft) high by 3.0 m (10 ft) wide. The general arrangement and coordinate system used are shown in Fig. 1. The "generating wing" is a semispan model attached to the tunnel scales with its trailing edge at the center of the tunnel turntable. Its measured lift curve (verified in this investigation) and more geometrical detail are available in Ref. 3. The "following wing" was mounted by means of a small fuselage to the tunnel traversing system (not shown) with its leading edge two generating-wing chord lengths downstream of the generating-wing trailing edge. This streamwise position was chosen to minimize the effects of vortex meander and to coincide with a position where a portion of the velocity field of the vortex had previously been measured.[4] While this close proximity to the generating wing is totally unrepresentative of the vortex hazard problem, minimizing meander and operating in a vortex whose structure is at least partially known greatly facilitated application of theoretical methods. Provision was made to pitch the following-wing-fuselage assembly relative to the traversing system.

There were actually two following-wing-fuselage assemblies of identical exterior shape but of different internal construction and instrumentation. One (the "force model") was fabricated of wood and fiberglass and was mounted to the traversing system through a force balance. The gages used to measure lift and rolling moment were calibrated in the tunnel. The estimated experimental uncertainty for a single measurement of lift is $\pm 5\%$ and for rolling moment $\pm 3\%$. The other assembly (the "pressure model") was fabricated of aluminum and was instrumented with 371 pressure taps distributed in chordwise rows on the upper and lower wing surfaces. The pressures were measured using differential transducers mounted in Scanivalve modules attached to the tunnel traversing mechanism aft of the model. The arrangement utilized allowed each transducer to be calibrated on each cycle of the associated Scanivalve.[2] The individual pressure lines were carefully leak checked at several stages in the construction of the model including after its final installation in the tunnel.

The mean position of the vortex in a given streamwise plane was determined using a dual-beam, two-color backscatter laser Doppler velocimeter (LDV) furnished by the Large-Scale Aerodynamics Branch at the NASA Ames Research Center. The two beams were positioned so that on the average they bracketed the vortex core and the mean vortex position was determined from knowledge of the LDV focus location.[4] The vortex was visualized using mineral-oil smoke.

In testing with the force model, the tunnel data acquisition system was used to record the balance output and freestream conditions at 100 different instants in time for each position of the wing relative to the mean vortex position. The results presented here are averages of these readings. With the pressure model, the pressure field on the entire wing was measured by cycling the Scanivalves once. This process was repeated on the order of 20 times to generate an average of the pressure at each point on the wing.

Test Conditions and Procedures

Vortex Structure

As previously mentioned, the streamwise position of the following wing was chosen to coincide with one of the measurement planes in an earlier study[4] of the structure of the tip vortex from this generating wing. In that study, a rapid-scanning LDV was used to obtain lateral traverses of tangential velocity through the vortex core.

Figure 2 shows the resulting profile (for $\alpha_G = 12$ deg, $V_\infty = 24$ m/s) in the transverse plane of interest here. In this figure, the tangential velocity (corrected for tunnel wall images) is normalized by the freestream velocity and the radial coordinate is normalized by the span of the generating wing. The center of the vortex is taken to be equidistant between the positions of maximum measured tangential velocity. A reasonable degree of symmetry is exhibited between the two sides of the traverse, except just at the edge of the core ($r/b_G \simeq 0.01$) and for $r/b_G \lesssim 0.08$. One may not, of course, infer any further degree of symmetry for the vortex from this, for this close to the wing one would expect neither that the vortex is axisymmetric nor that it is fully rolled up.[1,5-8] In fact, the small asymmetry noted at large r/b_G in Fig. 2 may be evidence of the unrolled-up portion of the wake.[7] The effects on the following wing of this unrolled-up

vortex sheet are apparent in some of the data acquired in this investigation but not presented here.[2]

Having duly noted that the vortex at this location is not axisymmetric, we will nevertheless proceed to represent its velocity distribution by two axisymmetric models. These models are used later as input to theoretical calculations of the lift and rolling moments induced on the following wing. This approach is dictated by a desire to determine the accuracy achievable by simple modeling, as well as by a lack of detailed data on the asymmetric structure. The two models are shown in Fig. 2. The first is a simple potential vortex with strength determined by fitting the experimental velocity distribution for $r/b_G > 0.02$. The second has vorticity distributed in accord with that in a two-dimensional, laminar, unsteady vortex (an "aged" vortex):

$$\Gamma/\Gamma_0 = 1 - \exp(-r^2/4\nu t) \tag{1}$$

This equation can be recast in the form

$$\frac{rV_\theta}{b_G V_\infty} = \left(\frac{\Gamma_0}{2\pi V_\infty b_G}\right)\left\{1 - \exp\left[-\left(\frac{r}{b_G}\right)^2\left(\frac{b_G^2}{4\nu t}\right)\right]\right\} \tag{2}$$

In applying this model, Γ_0, the circulation of the vortex at large r, is taken to be equal to the circulation of the potential vortex of the first model. The combination $b_G^2/4\nu t$ is chosen to provide best agreement to the experimental data in the vortical core region. As a result of these procedures, $\Gamma_0/2\pi V_\infty b_G = 9.68 \times 10^{-3}$ and $b_G^2/4\nu t = 1.052 \times 10^4$. It is of some interest to note that Γ_0 determined in this way is 77% of the value calculated from the maximum‡ section lift coefficient measured on this wing at $\alpha_G = 12$ deg[9]. This is suggestive of the extent of the rolling-up process at this streamwise location.

All data in the present investigation were taken with $V_\infty = 49$ m/s (160 fps), which corresponds to a dynamic pressure of 1.44 kPa (30 psf). The generating wing was always at $\alpha_G = 12.6$ deg. Because these values are somewhat different from the conditions used to generate the data of Fig. 2 ($V_\infty = 24$ m/s and $\alpha_G = 12$ deg), the constants just calculated must be adjusted before they are applied to the present situation. Because the roll-up process is essentially inviscid, no correction is applied for the change in Reynolds number (the V_∞ discrepancy). It is further assumed that the small (0.6 deg) discrepancy in α_G has no effect on the distribution of vorticity ($b_G^2/4\nu t$ unchanged), but that the effect on the total shed vorticity is linear in α_G. This leads to the final value, $\Gamma_0/2\pi V_\infty b_G = 10.14 \times 10^{-3}$.

Tests with the Force Model

As previously stated, the test arrangement was that shown in Fig. 1: generating-wing vertical at 12.6-deg angle of attack, following-wing horizontal at zero angle of attack. The following wing was moved in a constant transverse plane to different positions relative to the vortex by means of the tunnel traversing system and data were acquired as previously discussed.

To account for small imperfections in its construction, the loads on the force model were also obtained with the generating wing set to generate zero lift. For this measurement, the force model (still nominally at zero angle of attack) was located well above the wake of the generating wing. These loads ($\hat{C}_L = 0.0858$ and $\hat{C}_l = -0.00866$) were applied as tares to all of the other data from the force model. The resultant values (C_L, C_l) are thus induced solely by the presence of the vortex (under the assumption that for the positions occupied by the following wing, variations in the flow angularity in the freestream are small). The lift curve for the force model was also obtained.

‡This maximum c_l occurs for $0.35 \leq y/s \leq 0.60$.

Tests with the Pressure Model

As with the force model, the loads in the absence of the vortex were measured and all results corrected for these tare values. This process, when applied to the pressure at each tap location, results in C_p, the local pressure coefficient from which the effects of the wing thickness and any construction irregularities have been removed. The lift curve for the pressure model was also measured.

For each wing position, approximately 20 samples of the pressure at each pressure-tap location were recorded as described earlier. At each tap location, these values were averaged, converted to C_p, and integrated chordwise to define the span loading as follows:§

$$\begin{aligned} c_l &= \int_0^1 \frac{p_l - p_u}{q_\infty} \mathrm{d}\left(\frac{x}{c}\right) \\ &= \int_0^{0.05} \frac{p_l - p_u}{q_\infty} \mathrm{d}\left(\frac{x}{c}\right) + \int_{0.05}^{0.9} C_{p_l} \mathrm{d}\left(\frac{x}{c}\right) \\ &\quad - \int_{0.05}^{0.9} C_{p_u} \mathrm{d}\left(\frac{x}{c}\right) + \int_{0.9}^{1} \frac{p_l - p_u}{q_\infty} \mathrm{d}\left(\frac{x}{c}\right) \end{aligned} \tag{3}$$

The second and third terms on the right-hand side of this equation are evaluated by a straightforward numerical integration of the data using the trapezoidal rule. The fourth term provides a negligible contribution. The first term, however, provides a substantial contribution, although it involves only a small region in the wing which cannot be adequately instrumented with pressure taps in a model of this scale. Therefore, the contribution of this term was modeled by the relation

$$\int_0^{0.05} \frac{p_l - p_u}{q_\infty} \mathrm{d}\left(\frac{x}{c}\right) = k(C_{p_l} - C_{p_u})\Big|_{x/c=0.05} \tag{4}$$

where k was determined to be 0.0639 from two-dimensional section data for an NACA 0012 wing.[10] This procedure should be quite accurate over most of the wing as long as the local angle of attack induced by the vortex does not become too large.

Span loading as calculated by Eqs. (3) and (4) is integrated again to get the overall wing lift and rolling-moment coefficients.

Presentation and Discussion of Experimental Results

Following Wing in the Absence of the Vortex

In Fig. 3, the integrated lift coefficients for both the force and pressure models are shown as functions of angle of attack. With the exception of one apparently anomalous data point, the agreement for lift derived from the two models is good (within the uncertainty of the force data, ±5%). Predictions of the lift curve from a vortex-lattice program (described later) and from the method of Ref. 11 are shown for comparison and agree with the data to within this same order of accuracy. It is shown in Ref. 12 that for the low Reynolds number of this test ($Re_c = 330{,}000$) the lift curve becomes nonlinear for α greater than about 10 deg. The error bands on the data points from the force model show the standard deviation of those measurements. Because of the assumptions required to integrate the pressure data, accuracy of these data is best assessed by comparison to the force model data and to the theoretical estimates as is done in Fig. 3 for integrated lift coefficient. On a more detailed level, the span loading measured using the pressure model is also in good agreement with that calculated by the vortex-lattice program.

§This procedure cannot be applied at the fuselage location ($y/s = 0$). No c_l is calculated there.

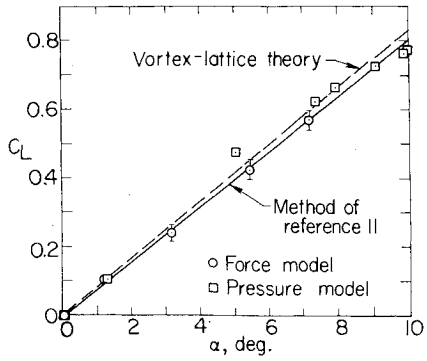

Fig. 3 Lift curve of the following wing.

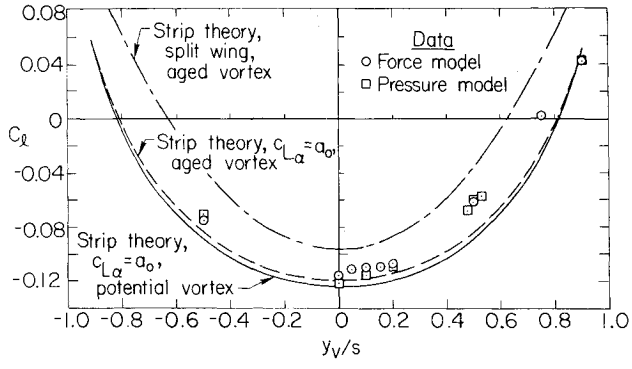

Fig. 4 Measured rolling-moment coefficient, $z_v/c=0.05$.

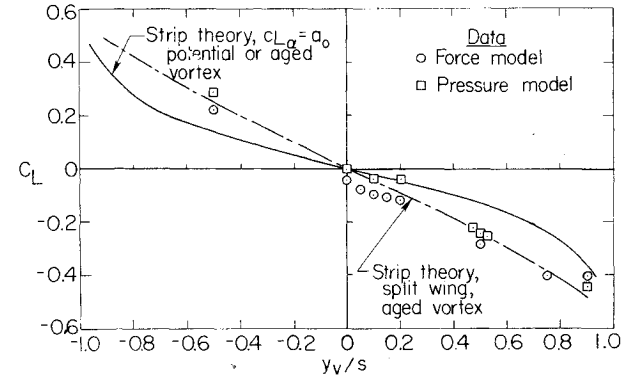

Fig. 5 Measured lift coefficient, $z_v/c=0.05$.

Following Wing in the Presence of the Vortex

For all of the data presented here, the vortex was at a single height above the wing but at different spanwise positions; that is, y_v/s varied for $z_v/c=0.05$. Notice that these quantities are the coordinates of the *unperturbed* position of the vortex relative to the wing. The presence of the wing causes the vortex to deflect so that its actual position over the wing is a function of the streamwise coordinate x. However, the unperturbed vortex position is most appropriate for input to and comparison with theoretical methods.

Measured rolling-moment coefficients are shown in Fig. 4; measured lift coefficients are shown in Fig. 5. Data from both the force and pressure models are included, as are some theoretical results discussed in the next section. These figures display reasonable agreement between the data from the different models, just as for the measurements shown previously for the case with no vortex present. The standard deviation of the measurements from the force model in the presence of the vortex is approximately represented by the symbol size in these figures. Note that this approximately bounds the effects of meander in these data.

The detailed pressure distributions obtained in this investigation (which result in the integrated values of Figs. 4 and 5) give evidence of the combined effects of nonlinear suction lift and vortex bending[2,13] near the vortex, and far from the vortex resemble standard section data. This latter observation suggests that the portions of the flowfield far from the vortex might be modeled in a straightforward fashion using strip theory. The success of this theoretical approach (and others) is assessed in the next section. Some detailed pressure distributions are presented in support of specific points.

III. Description of Theoretical Methods and Comparison with Data

Three standard methods of linear wing analysis (strip theory, vortex-lattice theory, and reverse-flow theory) are used to predict the loads on the wing due to the vortex. The boundary conditions used in these calculations consist of the induced velocity field from either a potential vortex or the "aged" vortex of Eq. (1), with the constants required for the description of the vortex structure determined as described earlier. The methods are applied assuming that the presence of the wing does not alter the vortex structure; that is, the vortex remains rectilinear and the incident velocity field is unchanged from that existing for the isolated vortex.

Strip Theory

Several versions of this simple approach have been applied to this problem in prior investigations, with varying claims of success.[1,7,14,15] Using strip theory, each infinitesimal element of the wing is considered to be independent of the others, and the load on each element is assumed to be calculable from the local section angle of attack. Thus, for a rectangular wing

$$C_L=\frac{1}{2s}\int_{-s}^{s} c_{L_\alpha}\frac{w_v}{V_\infty}\,dy \tag{5}$$

$$C_l=\frac{1}{4s^2}\int_{-s}^{s} c_{L_\alpha} y\frac{w_v}{V_\infty}\,dy \tag{6}$$

where c_{L_α} is the section lift-curve slope and w_v/V_∞ is the local section angle of attack. Previous applications of this method differ in the amount of empiricism used in the specification of c_{L_α} and w_v/V_∞.

In this section two versions of strip theory (differing in the treatment of c_{L_α}) are used to illustrate the fundamental features of the method. In the first version, c_{L_α} is assumed to be constant over the entire wing and equal to a_0, the three-dimensional lift-curve slope ($a_0=4.58/\text{rad}=0.08/\text{deg}$ is used, see Fig. 3). Both descriptions of the vortical velocity field developed earlier are used in conjunction with this asumption.

The second version of strip theory used here is based on the reasoning (set forth in Ref. 15) that the portions of the wing on either side of the vortex act as separate wings, each with its own (constant) value of lift-curve slope. The lift-curve slope for either portion of the wing is determined from

$$c_{L_\alpha}=\frac{2\pi\mathcal{R}}{P\cdot\mathcal{R}+2} \tag{7}$$

where $\mathcal{R}$ is the aspect ratio and P is the ratio of semiperimeter to span, each evaluated for the wing portion treated as a separate wing. In this second (split-wing) version of strip theory, the aged-vortex relation is used to describe the distribution of section angle of attack.

In Fig. 4 predictions of rolling moment are shown from the "whole-wing" and the "split-wing" versions of strip theory. The predictions shown ignore the effects of the image vortices present because of the tunnel walls. Inclusion of the closest eight of these images results in very small changes in the coefficients (0.002 in C_l, 0.01 in C_L); the effects of these images are therefore neglected in all subsequent calculations.

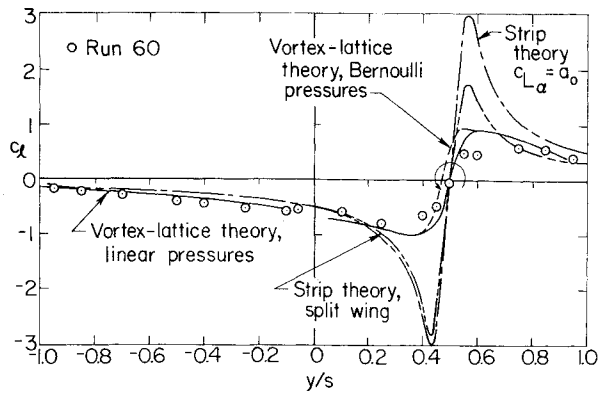

Fig. 6 Comparison of predicted and measured span loadings, $y_v/s = 0.5$ and $z_v/c = 0.05$. Predictions use rectilinear aged vortex.

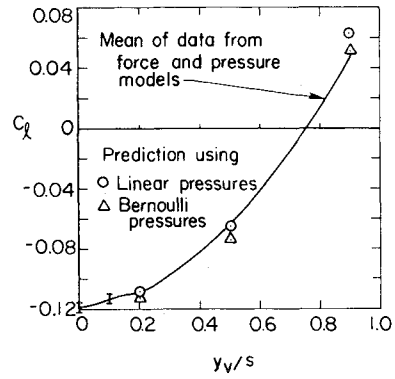

Fig. 7 Comparison with data of rolling-moment coefficient predicted by vortex-lattice theory using rectilinear aged vortex, $z_v/c = 0.05$.

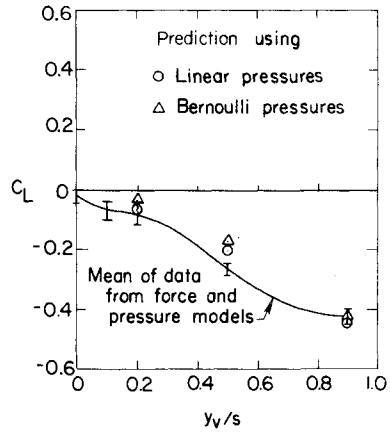

Fig. 8 Comparison with data of lift coefficient predicted by vortex-lattice theory using rectilinear aged vortex, $z_v/c = 0.05$.

It is seen that the best overall agreement with data is obtained for the approach which uses $c_{L_\alpha} = a_0$ for the whole wing in conjunction with the aged vortex. However, the agreement attained by this method is quite variable. Near $y_v/s = 0$, agreement within about 10% is attained; at $y_v/s = 0.5$, the discrepancy is nearly 40%; but at $y_v/s = 0.9$, there is excellent agreement. Examination of the lift coefficient results of Fig. 5 reveals a similarly varying level of agreement for this method. Here, however, the whole-wing method in conjunction with a potential vortex leads to virtually identical results, while the split-wing method exhibits considerably improved agreement with data for all y_v/s.

The reason for this seemingly erratic behavior is apparent from examination of the predicted and measured span loadings in Fig. 6. This figure shows a case where the agreement with data for rolling-moment coefficient from all of the versions of strip theory is poor. The (unperturbed) position of the vortex relative to the wing and the approximate core size are shown to scale. The span loadings predicted using the whole-wing and split-wing versions of strip theory and the aged vortex are shown; that from the whole-wing approach and the potential vortex, not shown, differs from the whole-wing, aged-vortex approach only in the immediate vicinity of the vortex where $|c_l|$ becomes very large. Predictions from vortex-lattice theory are also shown and are discussed later. It is clear that both versions of strip theory do a poor job of predicting the spanwise distribution of loading. This is particularly obvious near the vortex where the strong spanwise gradients invalidate the assumptions of no interference between adjacent strips. The same behavior is observed for vortex positions where strip theory gives good results for integrated coefficients. Therefore, where strip theory gives good results it is fortuitous. Compensating errors occur at different positions on the wing.

In the context of linear theory, there are two major possible sources for these (offsetting) errors. The first is that mutual interaction between adjacent wing sections is important. The second is that the aged vortex of Eq. (1) is a poor representation of the velocity field that exists when the vortex is close to the following wing; that is, the previously mentioned vortex deflection and possible bursting of the vortex are not represented by this model and may have strong effects on the induced loading. The first possible source of error is removed by applying vortex-lattice theory (or reverse-flow theory) to the problem using the aged-vortex representation, and assuming the vortex to be rectilinear. These approaches are now described. The second possible source of error is discussed subsequently.

Vortex-Lattice Theory – Rectilinear Vortex

The vortex-lattice method is an implementation of linear, potential theory wherein the wing and fuselage are represented by a network of distributed singularities. The particular implementation used in this work is described in Refs. 16 and 17. In the present work, it was found adequate to model each wing panel by 20 spanwise rows of 4 chordwise horseshoe vortices. The fuselage is modeled as a circular cylinder with diameter of 4.47 cm (1.75 in.) and its axis coincident with the x axis shown in Fig. 1. The image of the incident vortex in this cylinder is required to maintain the flow tangency condition on its surface; a second vortex at the axis of the cylinder is required to maintain the proper circulation at infinity.

Once the wing perturbation velocities are calculated by the linear theory of the vortex-lattice program, they can be used in any desired pressure-velocity relationship to calculate the surface pressures on the wing. These pressures are then integrated to get lift and rolling moment. It can be shown[2] that the contributions to surface pressure of the nonlinear terms present in the Bernoulli pressure relation are of the same order and of opposite sign from the contributions due to vortex bending. Therefore, in the present treatment of a rectilinear vortex, it is appropriate to use the linear pressure-velocity relation. However, for illustrative purposes, examples of loadings calculated from Bernoulli pressures are also included.

Integrated rolling moment and lift calculated in these ways are shown in Figs. 7 and 8; vortex-lattice calculations were made at $y_v/s = 0.2$, 0.5, and 0.9 and are represented by the plotted symbols. The solid lines in these figures pass through the mean of the pressure and force data from Figs. 4 and 5; the bands on these lines show the spread in data from the two models.

The level of agreement with the rolling-moment data in Fig. 7 is quite good, except with the vortex very near the wingtip. With the exception of that condition, the method using linear pressures is slightly better than that using Bernoulli pressures. The agreement for both methods with the lift data in Fig. 8 is of the same order as the agreement between data from the force and pressure models.

As before, examination of the distribution of loading can lend some insight into the behavior of the overall results. Returning to Fig. 6, we see the span loading for a case ($y_v/s=0.5$) where both linear and Bernoulli pressure calculations resulted in good agreement with rolling-moment data, with the linear pressure calculation doing slightly better. The improvement in span loading gained by accounting for mutual interaction between wing sections is immediately obvious by contrasting the agreement of either vortex-lattice approach to data with that of strip theory. It is seen that the loads are calculated quite well, except in the immediate vicinity of the vortex location. Using the Bernoulli relation leads to no particular improvement here. The agreement is slightly better on the left of the vortex, slightly worse on the right side.

Some further understanding of the level of agreement achieved by these vortex-lattice methods is derived by examining the most detailed output of these methods, surface-pressure coefficients. It is particularly instructive to compare the spanwise distribution of pressure at a constant chordwise position. Figures 9a and 9b show measured and calculated pressures due to the vortex on the top and bottom wing surfaces, respectively, for $y_v/s=0.5$, $z_v/c=0.05$. The measured pressures are for $x/c=0.65$. The calculated pressures are for $x/c=0.688$. In this region of the wing, this small discrepancy in chordwise position is not important for the purposes of the present discussion. The pressure distributions on both surfaces emphasize again that the agreement with data achieved is good, except near the vortex. On the upper surface, the calculated suction peak (using Bernoulli pressures) is overemphasized and slightly mislocated, indicating that the vortex has in fact moved slightly to the right. On the lower wing surface (Fig. 9b), there is also a calculated and a measured suction peak. Here, however, the calculated peak is underemphasized and too far to the right. It is clear from these remarks that, while using the Bernoulli pressure relation does qualitatively represent some real effects in the calculation, its use in conjunction with the assumption of an unaltered vortex structure does not lead to improved agreement for loading over a calculation made using linear pressures and a rectilinear vortex. Improvement in the accuracy of prediction would seem to depend on an accurate representation of the effects of the wing on the vortex. The improvements to be gained, however, do not appear to warrant the effort required.

Reverse-Flow Theory

Under the assumption of a rectilinear vortex, reverse-flow theory[18,19] can be used to calculate the induced rolling moment, and the theory is equivalent to that of the preceding section. After an initial calculation of the span loading in the appropriate reverse flow, subsequent calculation of rolling moment for any vortex position is reduced to a simple quadrature. Although the loading distribution is not an output of this method, the calculation is of the same accuracy as that of the preceding section. Reverse-flow theory is therefore a very economic approach, as long as details of the loading are not required.

The reverse-flow relation for rolling moment is

$$C_l = -\frac{1}{4s^2}\int_{-s}^{s}\left(\frac{w_v}{V_\infty}\right)\left(\frac{V_\infty}{p}\right)(c_l)_{\text{roll}}\,dy \qquad (8)$$

where $(c_l)_{\text{roll}}$ is the span-loading distribution for the rectangular wing in steady roll at roll angular velocity p. Either vortex model can be used for w_v/V_∞. In this investigation, $(c_l)_{\text{roll}}$ was calculated using vortex-lattice theory and Eq. (8) was applied using w_v/V_∞ from the aged vortex. It was verified that the results from this approach are equivalent to those from vortex-lattice theory (using linear pressures).

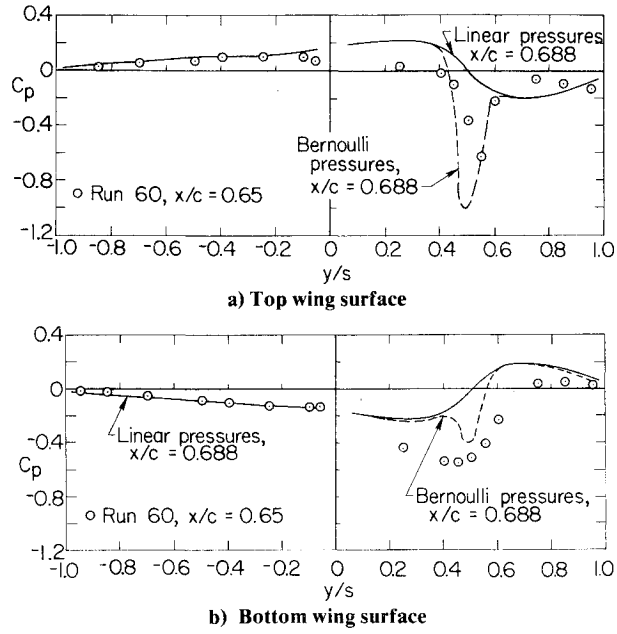

Fig. 9 Comparison with data of pressure coefficients predicted by vortex-lattice theory using rectilinear aged vortex, $y_v/s=0.5$ and $z_w/c=0.05$.

Some Remarks on Calculations Including Vortex Bending

As mentioned previously, for a point vortex, contributions to loading from vortex bending and nonlinear terms in the Bernoulli pressure relation are of the same order and of opposite sign. To achieve agreement improved over that demonstrated in the previous sections would therefore seem to require satisfactory modeling of vortex bending as well as inclusion of the Bernoulli terms.

The vortex-lattice program used in this investigation incorporates a vortex-tracking scheme based on slender-body theory. This scheme is a simplified version of the analysis for the cruciform wing case.[20,21] It is inappropriate for use here, however, because it does not take into account the upwash field ahead of the rectangular wing. This upwash field results in a large vertical deflection of the vortex, as observed in the wind tunnel. But even if a more complete tracking scheme were devised, it would not lead to fully satisfactory results for the case with the vortex very close to the wing. In this situation the vorticity is more widely distributed and neither the potential nor the aged vortex as used here is truly applicable; higher-order accuracy would require proper accounting for the full mutual interaction of the vortex and the wing.

This requirement is fortunately not of major concern. The accuracy achieved through the straightforward application of strictly linear analysis in conjunction with a rectilinear vortex model should be entirely satisfactory for most purposes.

IV. Concluding Remarks

This investigation has resulted in detailed measurements of the loads on a wing in close proximity to a tip vortex generated by a larger, upstream semispan wing. Good agreement of the integrated pressure measurements with overall loads measured by means of a force balance is attained.

The measurements show that over most of the wing the loads induced by the vortex are due to the spanwise varying angle of attack in the vortical flowfield. For a limited range of wing-vortex spacings, there are also contributions to the loading from vortex bending and the nonlinear terms in the Bernoulli pressure relation. It is demonstrated, however, that failure to model these last two effects results in only a small penalty in predictive accuracy.

Various theoretical methods were used to compute the induced loads. Straightforward applications of strip theory resulted in a varying level of agreement with the measurements. Comparison of the predicted and measured span loadings reveals uniformly poor accuracy, however, indicating that the limited success strip theory does achieve is fortuitous. In these comparisons, two models for the vortex velocity field were used; one a simple potential vortex, the other allowing for distributed vorticity in the core. Both models are based on previously published LDV traverses of the vortex of interest at the appropriate streamwise station. Allowance for the finite vortical core improved agreement slightly over calculations made with the potential vortex model.

Loads predicted using linearized pressures from vortex-lattice theory applied in conjunction with a rectilinear vortex model (with distributed vorticity) are within about 15% of measurements unless the vortex is very close to the wingtip. Agreement with measured span loadings is good except in the immediate vicinity of the vortex. The reverse-flow theorem which can be used to calculate overall loads to the same accuracy is presented.

The use of pressures calculated using the Bernoulli relation in conjunction with vortex-lattice theory and a rectilinear vortex does not result in improved agreement for loading although it does improve agreement for pressure distribution over part of the wing. Improvement in predictions should result from accounting for the interference of the wing on the vortex path, unless the wing is very close to the vortex. In this case, the resultant more widely distributed vorticity would have to be modeled.

In summary, economic predictions of overall loads of sufficient accuracy for most applications can be achieved by using reverse-flow theory. If the predictions are for cases where the vortex is within a core radius of the wing, a vortex model with a core should be used. If detailed loading distributions are required, fully linearized vortex-lattice theory gives good results. Significant improvements in accuracy beyond this situation are likely to be obtained only by accounting fully for mutual wing-vortex interference.

Acknowledgment

This work was sponsored by the NASA Ames Research Center under Contract NAS2-9398.

References

[1]Smith, W. G. and Lazzeroni, F. A., "Experimental and Theoretical Study of a Rectangular Wing in a Vortical Wake at Low Speed," NASA TN D-339, Oct. 1960.

[2]McMillan, O. J., Schwind, R. G., Nielsen, J. N., and Dillenius, M.F.E., "Rolling Moments in a Trailing Vortex Flow Field," NASA CR-151961, Feb. 1977.

[3]Spivey, W. A. and Duhon, J. M., "A Study to Investigate the Aerodynamics of Rotor Blade Tip Shapes," Bell Helicopter Company Rept. No. 299-099-468, Jan. 1970.

[4]Orloff, K. L. and Grant, G. R., "The Application of Laser Doppler Velocimetry to Trailing Vortex Definition and Alleviation," NASA TM X-62, 243, Feb. 1973.

[5]Fage, A. and Simmons, L.F.G., "An Investigation of the Air-Flow Pattern in the Wake of an Aerofoil of Finite Span," *Philosophical Transactions*, Ser. A, Vol. 225, Jan. 1926, pp. 303-330.

[6]El-Ramly, Z., Rainbird, W. J., and Earl, D. G., "Some Wind Tunnel Measurements of the Trailing Vortex Development Behind a Swept-Back Wing: Induced Rolling Moments on Intercepting Wings," AIAA Paper 75-884, AIAA 8th Fluid and Plasma Dynamics Conference, Hartford, Conn., June 1975.

[7]El-Ramly, Z., "Investigation of the Development of the Trailing Vortex System Behind a Swept-Back Wing," Carleton University, Rept. No. ME/A 75-3, Oct. 1975.

[8]El-Ramly, Z. and Rainbird, W. J., "Computer Controlled System for the Investigation of the Flow Behind a Swept-Back Wing," *Proceedings, AIAA 9th Aerodynamic Testing Conference*, June 1976, pp. 119-128.

[9]Chigier, N. A. and Corsiglia, V. R., "Tip Vortices-Velocity Distributions," Preprint No. 522, 27th Annual National V/STOL Forum of the American Helicopter Society, May 1971.

[10]Riegels, F. W., *Aerofoil Sections*, Butterworths, London, 1961, p. 201.

[11]DeYoung, J. and Harper, C. W., "Theoretical Symmetric Span Loading at Subsonic Speeds for Wings Having Arbitrary Plan Form," NACA Rept. No. 921, 1948.

[12]Jacobs, E. N. and Sherman, A., "Airfoil Section Characteristics as Affected by Variations of the Reynolds Number," NACA Rept. No. 586, June 1936.

[13]Patel, M. H. and Hancock, G. J., "Some Experimental Results of the Effect of a Streamwise Vortex on a Two-Dimensional Wing," *Aeronautical Journal*, Vol. 78, April 1974, pp. 151-155.

[14]Iversen, J. D. and Berstein, S., "Trailing Vortex Effects on Following Aircraft," *Journal of Aircraft*, Vol. 11, Jan. 1974, p. 60.

[15]Rossow, V. J., Corsiglia, V. R., Schwind, R. G., Frick, J.K.D., and Lemmer, O. J., "Velocity and Rolling-Moment Measurements in the Wake of a Swept-Wing Model in the 40- by 80-Foot Wind Tunnel," NASA TM X-62414, April 1975.

[16]Spangler, S. B. and Dillenius, M.F.E., "Investigation of Aerodynamic Loads at Spin Entry," Office of Naval Research, Rept. ONR-CR212-225-2, May 1976.

[17]Spangler, S. B. and Nielsen, J. N., "Exploratory Study of Aerodynamic Loads on a Fighter-Bomber at Spin Entry," Nielsen Engineering & Research, Mountain View, Calif., NEAR TR 87, May 1975.

[18]Heaslet, M. A. and Spreiter, J. R., "Reciprocity Relations in Aerodynamics," NACA Rept. 1119, 1953.

[19]Nielsen, J. N., *Missile Aerodynamics*, McGraw-Hill, New York, 1960, pp. 221-222.

[20]Nielsen, J. N., Hemsch, M. J., and Dillenius, M.F.E., "Further Studies of the Induced Rolling Moments of Canard-Cruciform Missiles as Influenced by Canard and Body Vortices," Nielsen Engineering & Research, Mountain View, Calif., NEAR TR 79, Jan. 1975.

[21]Nielsen, J.N., Spangler, S.B., and Hemsch, M.J., "A Study of Induced Rolling Moments for Cruciform-Winged Missiles," Nielsen Engineering & Research, Mountain View, Calif., NEAR TR 61, Dec. 1973.